arXiv:2305.17354v2 [physics.flu-dyn] 19 Jul 2023

Linking turbulent waves and bubble diffusion in self-aerated open-channel flows: Two-state air concentration

Matthias Kramer[1]†, Daniel Valero [2,3]

[1]UNSW Canberra, School of Engineering and Information Technology (SEIT), Canberra, ACT 2610, Australia

[2]Karlsruhe Institute of Technology (KIT), Institute for Water and River Basin Management (IWG), Karlsruhe, Germany

[3]IHE Delft, Water Resources and Ecosystems dept., Delft, the Netherlands

High Froude-number flows become self-aerated when the destabilizing effect of turbulence overcomes gravity and surface tension forces. Traditionally, the resulting air concentration profile has been explained using single-layer approaches that invoke solutions of the advection-diffusion equation for air in water, i.e., bubbles' dispersion. Based on a wide range of experimental evidences, we argue that the complete air concentration profile shall be explained through the weak interaction of different canonical turbulent flows, namely a Turbulent Boundary Layer (TBL) and a Turbulent Wavy Layer (TWL). Motivated by a decomposition of the streamwise velocity into a pure wall flow and a free-stream flow [Krug et al., J. Fluid Mech. vol. 811, 2017, pp. 421–435], we present a physically consistent two-state formulation of the structure of a self-aerated flow. The air concentration is mathematically built upon a modified Rouse profile and a Gaussian error function, resembling vertical mass transport in the TBL and the TWL. We apply our air concentration theory to over 500 profiles from different data sets, featuring excellent agreement. Finally, we show that the turbulent Schmidt number, characterizing the momentum-mass transfer, ranges between 0.2 to 1, which is consistent with previous mass-transfer experiments in TBLs. Altogether, the proposed flow conceptualization sets the scene for more physically-based numerical modelling of turbulent mass diffusion in self-aerated flows.

† Email address for correspondence: m.kramer@adfa.edu.au

1. Introduction

In a supercritical open-channel flow, turbulent stresses next to the free-surface can be large enough to overcome surface tension and gravity effects, thus leading to air bubble entrainment (Brocchini and Peregrine 2001; Valero 2018) and their subsequent breakdown (Deane and Stokes 2002; Chan et al. 2021). This process is called self-aeration (Fig. 1a), and the location of the so-called inception point of air entrainment has been associated with the interaction of a developing boundary layer with the free-surface (Lane 1939; Straub and Anderson 1958; Wood 1984), as well as with an unstable state of free-surface perturbations (Brocchini and Peregrine 2001; Valero 2018). Air–water multiphase flows are of key interest because entrained air affects flow properties, thereby leading to (i) flow bulking, which may compromise overtopping safety of spillways (Straub and Anderson 1958; Hager 1991; Boes 2000), (ii) drag reduction, which can lead to flow velocities of twice or thrice the counter-part single-phase flow (Wood 1984; Chanson 1994; Kramer et al. 2021), (iii) cavitation protection of solid surfaces (Falvey 1990; Frizell et al. 2013), (iv) enhanced gas transfer (Gulliver et al. 1990; Bung 2009), and (v) total dissolved gas super-saturation that can mortally affect fish (Pleizier et al. 2020). Therefore, the accurate description of the air concentration distribution has been a topic of sustained research interest since the second half of the twentieth century, and two different schools of thought can be distinguished (Fig. 1b).

The first group of researchers conceptualized the air concentration distribution using a single-layer approach, thus assuming a "homogeneous" mixing process between the channel bottom and y_{90}, except Valero and Bung (2016), who described air concentrations within a turbulent-wavy region. Here, y_{90} is the flow depth where the time-averaged air concentration is $\overline{c} = 0.9$, with $\overline{c}$ being defined as volume of air per volume of air-water mixture. Rao and Gangadharaiah (1971) and Wood (1984) derived expressions for the air concentration distribution based on mass conservation considerations, while Chanson (1995), Chanson and Toombes (2001), and Zhang and Chanson (2017) presented solutions of the advection-diffusion equation for air in water under the assumption of variable turbulent diffusivity across the water depth (up to y_{90}). We argue that the assumption of a "homogeneous" bubbly air-water mixture does not contemplate the real structure of a self-aerated flow, as depicted in Fig. 1a, although we acknowledge that single-layer approaches can show a good data-driven agreement with typical S-shaped concentration profiles, which is however at the expense of empirically fitted coefficients.

Based on flow visualization, Killen (1968) discerned several distinct flow regions of a self-aerated flow (Fig. 1a), comprising:

   (i) a single-phase (water) region next to the channel bottom (not always present),
  (ii) a bubbly flow region,
 (iii) a free-surface region, characterised by free-surface perturbations/waves,
 (iv)   and a spray/droplet region.

Wilhelms and Gulliver (2005) identified that measured air concentrations typically comprise entrained air in the form of bubbles and entrapped air between surface roughness/waves, corresponding to regions (ii) and (iii), while very fine droplets, forming region (iv), have only been observed at prototype scale and in near-full-scale facilities (see Table 1 of Hohermuth et al. 2021; Bai et al. 2022). Further, it is known that the single-phase region (i) vanishes for depth-averaged (mean) air concentrations $\langle \overline{c} \rangle \gtrless 0.25$, which is because the bubbly flow layer protrudes to the channel bottom (Straub and Anderson 1958; Hager 1991; Wei et al. 2022). Here, the mean air concentration is defined as:

$$\langle \overline{c} \rangle = \frac{1}{y_{90}} \int_{y=0}^{y_{90}} \overline{c} \, \mathrm{d}y \tag{1.1}$$
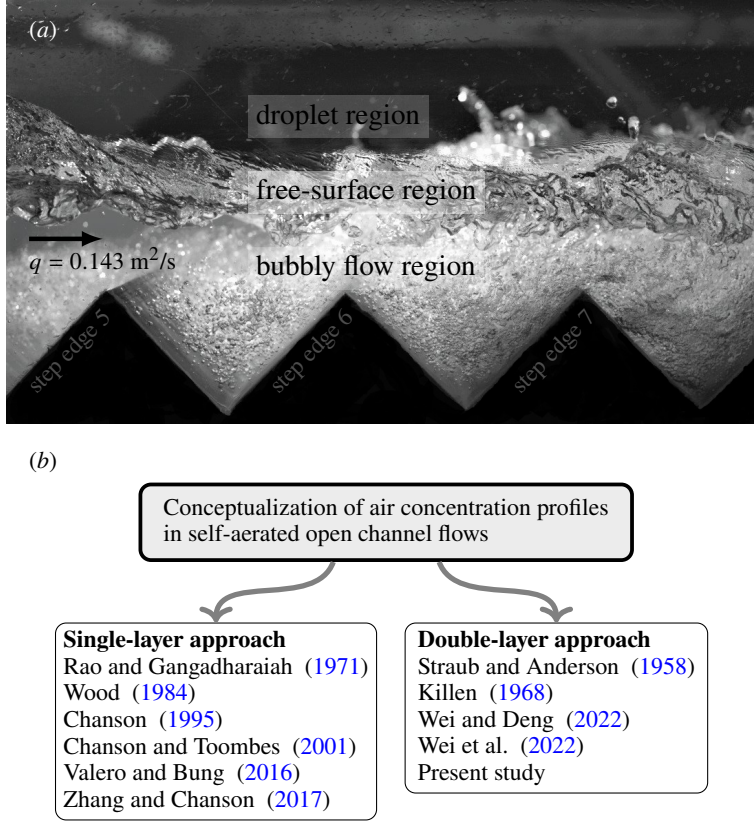
Figure 1: Characteristic regions and modelling approaches of self-aerated open-channel flows (*a*) snapshot of the self-aerated flow down a stepped chute (The University of Queensland) with clear distinction of the bubbly flow region and the wavy free-surface region; specific water discharge $q = 0.143$ m²/s, chute angle $\theta = 45°$; step edges 5 to 7 (*b*) schools of thought in the modelling of air concentration distributions in self-aerated flows

where y is the bed-normal coordinate with $y = 0$ at the channel invert.

The second group of researchers differentiated between the aforementioned regions using multi-layer approaches, mostly in the form of double-layer models (Fig. 1*b*), such as those from Straub and Anderson (1958) and Killen (1968), consisting of a lower layer where air bubbles are transported by turbulence throughout the flow, and an upper layer with a heterogeneous mixture of water droplets ejected from the flowing stream. The transition point between the two regions, defined by the depth $y_\star$ with corresponding air concentration $\overline{c}_\star$, was determined based on the maximum gradient $(d\overline{c}/dy)_{max}$ by Straub and Anderson (1958). In contrast, Wei and Deng (2022) argued that the flow depth y_{50}, i.e., the depth where $\overline{c} = 0.5$, can be used as interior transition depth, and Wei et al. (2022) proposed some additive concepts to model the air concentration distribution. Generally, a double-layer (or multi-layer) approach better reflects the physical nature of an air-water flow, but an in-depth understanding of the flow transition is currently missing. Furthermore, none of the double-layer models has established a link between the air concentration and the velocity distribution, i.e., a coupling of mass and momentum transfer.
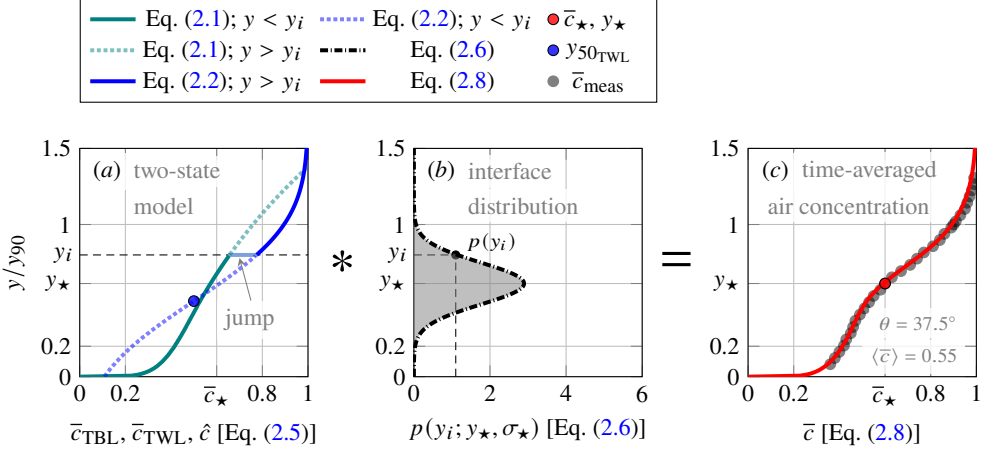
Figure 2: Two-state model for air concentration distribution (*a*) representation of the TBL air concentration [teal line, Eq. (2.1)], TWL air concentration [blue line, Eq. (2.2)], interface position y_i, and two-state model $\hat{c}$ (*b*) probability distribution of interface position, centered around $y_\star$ (*c*) comparison of the convoluted profile (convolution operation indicated by the $*$ symbol) with data from Straub and Anderson (1958, specific discharge $q = 0.322$ m^2/s; streamwise position $x = 13.88$ m)

Here, we propose a novel double-layer conceptualization of the air transport, which builds on two canonical flow layers of momentum, namely a Turbulent Boundary Layer (TBL) and a Turbulent Wavy Layer (TWL). We note that the TBL and the TWL conceptually feature a log-law and a constant free-stream velocity distribution, respectively. The air concentration of these layers is modelled using a modified Rouse profile (TBL, corresponds to regions i and ii) and a Gaussian error function (TWL, corresponds to region iii), both layers being convoluted using a two-state-principle, which is detailed in § 2. Through analysis of concentration profiles from literature, we show that the transition between TBL and TWL is closely linked to the boundary layer thickness (δ), and that other model parameters, such as the Rouse number (Rouse 1961; Dey 2014), are unequivocally determined by the mean air concentration (§ 3). For $\langle \overline{c} \rangle \lessapprox 0.25$, the Gaussian error function alone is able to predict the measured air concentration distributions, which suggests that entrapped air (within wave troughs) is prevalent in those flows. In § 4, we quantify the turbulent Schmidt number for aerated flows, followed by a discussion on model limitations.

2. Methodology: Two-state air concentration

The general principle of decomposing the streamwise velocity profile (and other flow statistics) into a pure wall flow state and a free-stream state was first introduced by Krug et al. (2017). Here, we hypothesize that the two-state concept can be extended to describe turbulent mass transport, such as the air concentration distribution in supercritical open-channel flows (Fig. 2). In the following, we seek expressions for the air concentration distribution within the TBL and the TWL.

2.1. *Air concentration within the TBL*

We note that the TBL features a log-law velocity distribution and turbulent air bubble diffusion. Assuming a parabolic distribution of turbulent diffusivity ($D_{t,y}$) up to half the boundary layer thickness, as well as a constant turbulent diffusivity for $y > \delta/2$ (also known as

parabolic-constant diffusivity distribution), we obtain a modified Rouse equation by solving the advection-diffusion equation for air in water. The expression for the air concentration $\overline{c}_{\mathrm{TBL}}$ within the TBL reads (Appendix A, Fig. 2a):

$$\overline{c}_{\mathrm{TBL}} = \begin{cases} \overline{c}_{\delta/2} \left(\frac{y}{\delta - y} \right)^{\beta}, & y \leqslant \delta/2 \\ \overline{c}_{\delta/2} \, \exp \left(\frac{4\beta}{\delta} \left(y - \frac{\delta}{2} \right) \right), & y > \delta/2 \end{cases} \tag{2.1}$$

where $\overline{c}_{\delta/2}$ is the air concentration at half the boundary layer thickness, $\overline{v}_r$ is the bed-normal bubble rise velocity, κ is the van Kármán constant, u_* is the friction velocity, and $\beta = \overline{v}_r S_c / \kappa u_*$ is a modified Rouse number, which encapsulates the turbulent Schmidt number S_c, the latter defined as the ratio of eddy viscosity and turbulent mass diffusivity. Here, we adopt the classical definition of the boundary layer thickness as the bed-normal distance at which 99% of the free-stream velocity is attained, as well as a constant value of $\kappa = 0.41$, while we acknowledge that slightly different values of the von Kármán constant have been discussed (Nagib and Chauhan 2008; Marusic et al. 2010; Morill et al. 2017).

2.2. *Air concentration within the TWL*

We emphasize that the air concentration of the TWL comprises surface waves/perturbations (entrapped air) as well as some entrained air bubbles. An analytical solution for the air concentration $\overline{c}_{\mathrm{TWL}}$ involves the Gaussian error function (Valero and Bung 2016); (Fig. 2a):

$$\overline{c}_{\mathrm{TWL}} = \frac{1}{2} \left(1 + \mathrm{erf} \left(\frac{y - y_{50_{\mathrm{TWL}}}}{\sqrt{2} \, \mathcal{H}} \right) \right) \tag{2.2}$$

where $y_{50_{\mathrm{TWL}}}$ is the mixture flow depth where the free-surface air concentration is $\overline{c}_{\mathrm{TWL}} = 0.5$, $\mathcal{H}$ is a characteristic length-scale that describes the thickness/height of the aerated wavy layer, and erf is the Gaussian error function. In single-phase flows, $\mathcal{H}$ is defined as the the root mean square wave height (Valero and Bung 2016). The air concentration of the TWL results from a superposition of entrapped air, transported between wave crests and troughs, and entrained air in the form of air bubbles travelling within the waves (Killen 1968; Wilhelms and Gulliver 2005). Because the volume of entrapped air within the TWL is typically much larger than the volume of entrained air, $\mathcal{H}$ still provides a clear indication of the root mean square wave height. However, for the sake of accuracy, we hereafter refer to $\mathcal{H}$ as length-scale of the TWL.

2.3. *Two-state convolution*

Consistent with the two-state formulation of Krug et al. (2017), we introduce the concept of an interface position y_i separating TBL and TWL. The air concentration profile $\hat{c}$ is defined for every position of y_i:

$$\hat{c} = \begin{cases} \overline{c}_{\mathrm{TBL}} \ (\text{Eq. 2.1}), & y \leqslant y_i \\ \overline{c}_{\mathrm{TWL}} \ (\text{Eq. 2.2}), & y > y_i \end{cases} \tag{2.3}$$

Using the Heaviside step function:

$$H(y - y_i) = \begin{cases} 0, & y - y_i \leqslant 0 \\ 1, & y - y_i > 0 \end{cases} \tag{2.4}$$

we can write Eq. (2.3) as follows:

$$\hat{c} = \overline{c}_{\mathrm{TBL}}(1 - H) + \overline{c}_{\mathrm{TWL}} H \tag{2.5}$$

Equations (2.3) and (2.5) correspond to the discontinuous profile shown in Fig. 2*a*, i.e., the two-state model. It is implied that the flow below the interface level y_i is fully explained by turbulent air bubble diffusion, whereas turbulent waves describe the air concentration above y_i. The interface position is now assumed to follow a random independent process, which is governed by a Gaussian probability distribution, shown in Fig. 2*b*:

$$p(y_i; y_\star, \sigma_\star) = \frac{1}{\sigma_\star \sqrt{2\pi}} \exp\left(\frac{-(y_i - y_\star)^2}{2\sigma_\star^2}\right) \tag{2.6}$$

where the transition depth $y_\star$ can be interpreted as the time-averaged y-location of the interface, and $\sigma_\star$ describes the standard deviation of y_i. To obtain a complete, time-averaged expression for the double-layer air concentration (Fig. 2*c*), we convolute $\hat{c}$ [Eq. (2.5)] with the interface probability p [Eq. (2.6)], which leads to (Krug et al. 2017):

$$\overline{c}(y) = \int_{-\infty}^{\infty} \hat{c} p \, dy_i = \overline{c}_{\text{TBL}} \int_{-\infty}^{\infty} (1 - H) p \, dy_i + \overline{c}_{\text{TWL}} \int_{-\infty}^{\infty} H p \, dy_i \tag{2.7}$$

where $\overline{c}_{\text{TBL}}$ and $\overline{c}_{\text{TWL}}$ are independent of y_i, thus allowing to simplify:

$$\overline{c}(y) = \overline{c}_{\text{TBL}}(1 - \Gamma) + \overline{c}_{\text{TWL}}\Gamma \tag{2.8}$$

with:

$$\Gamma(y; y_\star, \sigma_\star) = \frac{1}{2}\left(1 + \text{erf}\left(\frac{y - y_\star}{\sqrt{2}\sigma_\star}\right)\right) \tag{2.9}$$

We note that the lower limit of the integral in Eq. (2.7) was extended to $-\infty$, which however did not affect the results as $p(y_i < 0) \ll 1$. From a physical point of view, the convolution can be interpreted as a weighted-averaging operation, which lumps concentration discontinuities between TBL and TWL, such as the jump shown in Fig. 2*a*, into a smooth, continuous profile. At last, the interface distribution of the two-state model is not expected to be the same as the turbulent/non-turbulent interface (TNTI) in turbulent boundary layers, see discussion in Krug et al. (2017).

2.4. *Determination of model parameters*

The convoluted two-state air concentration model [Eq. (2.8)] has four free physical parameters, including the Rouse number (β), the length-scale of the TWL ($\mathcal{H}$), and two transition/interface parameters ($y_\star$, $\sigma_\star$). We note that the parameters δ, $\overline{c}_{\delta/2}$, and $y_{50_{\text{TWL}}}$ are regarded as fixed, as they are directly available from measurements. The free model parameters were derived through a two-step fitting procedure to an extensive experimental dataset of air concentration profiles. It is noted that both layers (TBL and TWL) allowed for an independent (simultaneous) fit away from the mean interface position $y_\star$, thus preserving the physical significance of their parameters.

In a first step, the Rouse number β was obtained by minimizing the sum of squared differences between measurements up to $\delta/2$ and Eq. (2.1). Here, the boundary layer thickness was computed from measured velocities; if such velocity measurements were not available, we assumed $\delta = 1.25\, y_\star$ (see § 3.2). At the same time, the length-scale $\mathcal{H}$ was obtained by minimizing the sum of squared differences between measurements and modelled air concentrations within the upper flow region. We note that $y_{50_{\mathrm{TWL}}}$ corresponds to y_{50}, which is a physical quantity that can be directly measured. However, this was not the case for 46 out of 571 re-analysed profiles with $\langle \overline{c} \rangle \gtrapprox 0.5$, where $y_{50_{\mathrm{TWL}}}$ was also obtained through fitting; in this case, the number of free parameters increased by one. In a second step, the mean interface position $y_\star$ was determined at the location where Eq. (2.2) departed from the measured air concentrations, which yielded better results when compared to using the maximum gradient $(\mathrm{d}\overline{c}/\mathrm{d}y)_{\mathrm{max}}$. Subsequently, the standard deviation $\sigma_\star$ of the interface position was determined using a best-fit approach.

3. Results

We apply our air concentration model to 571 concentration profiles from different data sets, as presented in the supplementary material (available at https://doi.org/10.1017/jfm.2023.440), comprising smooth chute data from Straub and Anderson (1958, 74 profiles), Killen (1968, 17 profiles), Bung (2009, 28 profiles), Severi (2018, 261 profiles), and stepped chute data from Bung (2009, 151 profiles), Zhang (2017, 6 profiles), and Kramer and Chanson (2018, 34 profiles). The terms "smooth" and "stepped" chute are commonly used in accordance with different roughness heights (k_s) of chute inverts, see Fig. 1 for an example of a stepped macro-roughness. The category "smooth" also comprises micro-rough inverts, and laboratory spillways are often considered as micro-rough for $k_s \gtrapprox 0.1$ mm (Felder et al. 2023). We note that this description slightly differs from the classic smooth/rough classification of wall flows (Pope 2000, Ch. 7).

3.1. *Representative application*

We demonstrate the application of our theory using a seminal series of measurements by Straub and Anderson (1958), who sampled air concentrations in the uniform region of a smooth chute ($k_s = 6.1$ mm) for chute angles from $\theta = 7.5°$ to $75°$, covering a wide range of flow rates from $q = 0.13$ to 0.92 m²/s. These measurements remain one of the most comprehensive and complete data sets to date, allowing us to illustrate the relative importance of each of the two states considered.

Figure 3 shows measured air concentrations from Straub and Anderson (1958) for $q = 0.322$ m²/s, together with the theoretical air concentration profiles of the TBL, TWL, and their convolution through the two-state model. For mean air concentrations $\langle \overline{c} \rangle \lessapprox 0.25$ (Fig. 3a), entrained air bubbles did not reach the channel bottom and aeration was mostly confined to the TWL. Such flows are dominated by entrapped air (free surface perturbations and turbulent waves), and the air concentration was well described by Eq. (2.2), see discussion in Felder et al. (2023). For larger $\langle \overline{c} \rangle$ (Figs. 3b - h), the air concentration of the TWL (indicated as blue line) deviated from the measurements at the transition point. Here, the two-state model [Eq. (2.8)] excellently detailed the air concentration measurements, and the corresponding model parameters are presented in Table 1.
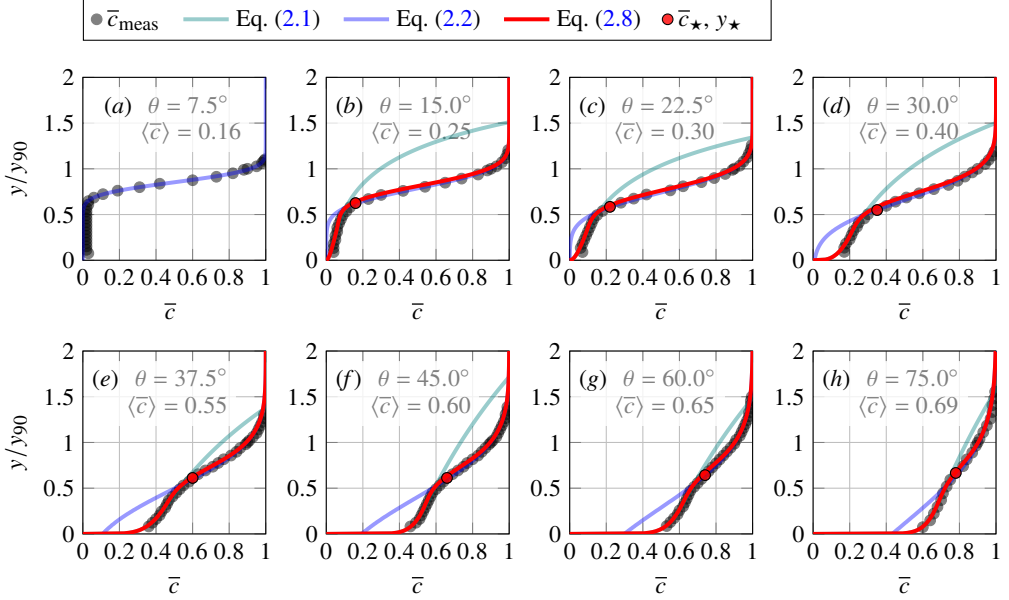
Figure 3: Measured air concentration distributions in flows down a laboratory smooth chute; data from Straub and Anderson (1958, q = 0.322 m^2/s; x = 13.88 m) (a - h) comparison of Eqns. (2.1), (2.2), and (2.8) with measurements

Table 1: Normalized parameters of the two-state convolution model for profiles shown in Fig. 3; as no detailed velocity measurements were available from Straub and Anderson (1958), we determined $y_\star$ first, and subsequently assumed $\delta = 1.25 y_\star$ (see § 3.2); measurements taken at x = 13.88 m from the flume inlet

sub-figure	q	x	θ	$\langle\overline{c}\rangle$	β	$\overline{c}_{\delta/2}$	$\delta/y_\star$	$y_{50_{\text{TWL}}}/y_{90}$	$\mathcal{H}/y_{90}$	$y_\star/y_{90}$	$\sigma_\star/\delta$
(-)	(m^2/s)	(m)	(°)	(-)	(-)	(-)	(-)	(-)	(-)	(-)	(-)
(a)	0.32	13.88	7.5	0.16	-	-	-	0.85	0.11	-	-
(b)	0.32	13.88	15.0	0.25	0.50	0.06	1.25	0.79	0.17	0.63	0.11
(c)	0.32	13.88	22.5	0.30	0.43	0.11	1.25	0.74	0.21	0.58	0.12
(d)	0.32	13.88	30.0	0.40	0.27	0.24	1.25	0.65	0.28	0.59	0.13
(e)	0.32	13.88	37.5	0.55	0.14	0.47	1.25	0.48	0.42	0.61	0.13
(f)	0.32	13.88	45.0	0.60	0.09	0.56	1.25	0.39	0.48	0.61	0.15
(g)	0.32	13.88	60.0	0.65	0.09	0.64	1.25	0.27	0.56	0.64	0.17
(h)	0.32	13.88	75.0	0.69	0.07	0.70	1.25	0.06	0.72	0.67	0.2

3.2. *Profile transition*

Next, we focus our attention on the flow transition between TBL and TWL. Figures 4a,b show a measured air concentration profile within the flow centreline of a stepped chute, together with the corresponding streamwise interfacial velocities ($\overline{u}$) and fluctuations from Kramer and Chanson (2018). Here, u'_{rms} is the root mean square of velocity fluctuations and $\overline{u}_{\text{max}}$ is the free-stream velocity. The chute angle was $\theta = 45°$ and measurements were taken at step edge 11, at a specific flow rate of $q = 0.067$ m^2/s. The transition depth $y_\star$ (or mean interface position) was determined through the procedure described in § 2.4 and is shown in Fig. 4a.
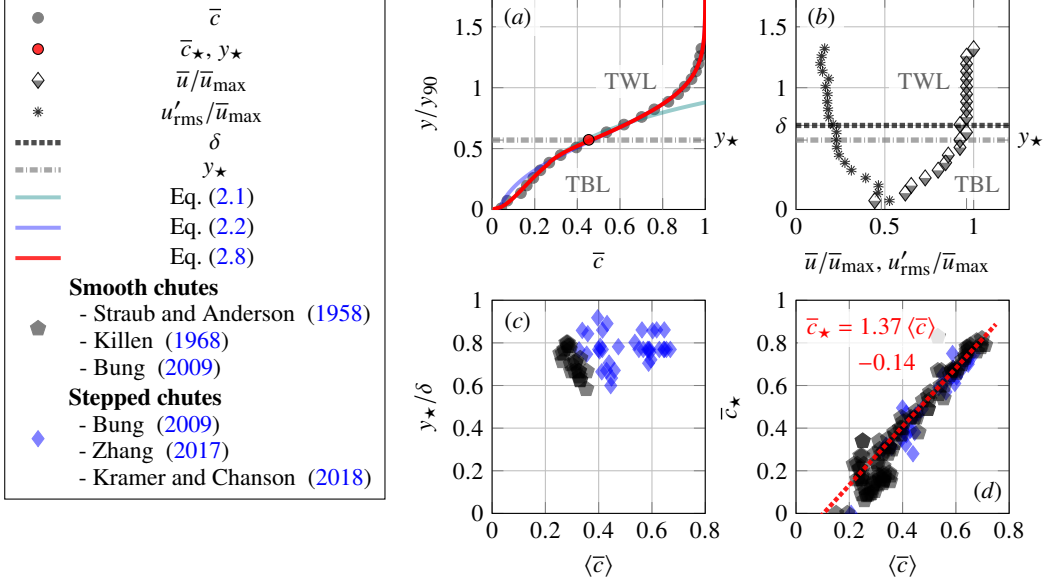
Figure 4: Determination of the transition point parameters $y_\star$ and $c_\star$ (a) exemplary air concentration profile, measured within the flow down a stepped spillway; $\theta = 45°$; $q = 0.067$ m^2/s; step edge 11 (b) corresponding normalised velocity profile and velocity fluctuations in bed-normal direction (c) ratio of $y_\star$ and boundary layer thickness δ (d) air concentration at transition point versus mean air concentration

A comparison of Figs. 4a,b, confirms that the layer below $y_\star$ (i.e., mainly TBL) was characterised by high flow shearing, whereas the layer above $y_\star$ (TWL) corresponds to a uniform free-stream velocity, and, in this instance, the ratio between the transition depth and the boundary layer thickness is $y_\star/\delta = 0.83$. This finding supports our hypothesis that the air concentration distribution is intrinsically connected to the flow momentum layers, both separated by a fluctuating TBL - TWL interface. We find that $y_\star/\delta$ ranges between 0.6 and 0.9 (Fig. 4c), which is consistent with interface positions reported in Krug et al. (2017). The dimensionless standard deviation of the interface position remains constant at $\sigma_\star/\delta = 0.1$ to 0.2, which yields a good description of all concentration profiles. Our expression for $\sigma_\star$ assumes that the interface position y_i is linked to the underlying TBL edge, while we consider that the waves/perturbations of the TWL – described via $\mathcal{H}$ – are a reflection of that turbulent process. Figure 4d shows that the air concentration at the transition point is linearly dependent on the mean air concentration, and can be estimated through the empirical relationship $\overline{c}_\star = 1.37 \langle \overline{c} \rangle - 0.14$, valid for smooth and stepped chutes.

Finally, we acknowledge the scatter in Fig. 4c, which likely stems from measurement uncertainties of dual-tip phase-detection probes related to air concentration and interfacial velocity (Kramer et al. 2020; Hohermuth et al. 2021). We also note that the smooth chute data of Straub and Anderson (1958); Killen (1968); Severi (2018) were not added to Fig. 4c, which is because no velocity information was available or because flows were dominated by entrapped air, implying that no profile transition occurred.
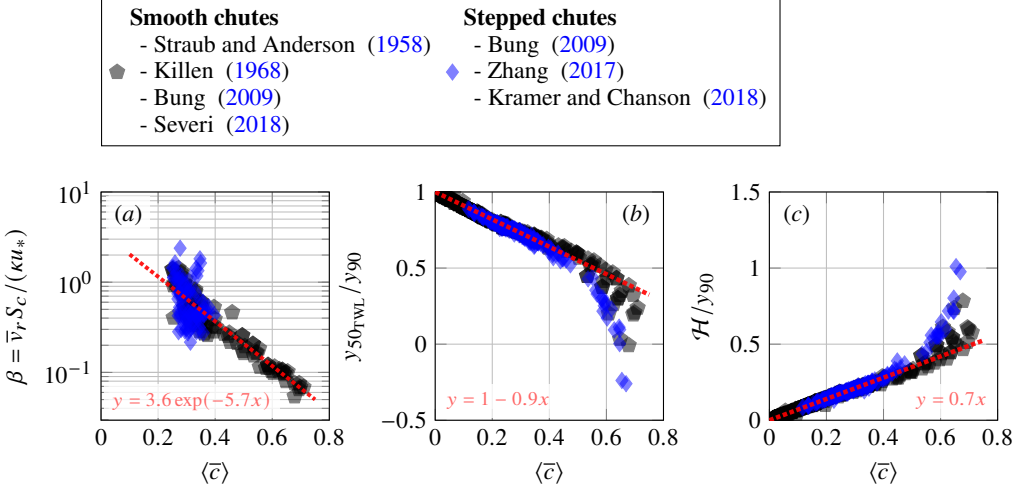
Figure 5: Model parameters are a function of the mean air concentration: (*a*) Rouse number β (*b*) relation of TWL mixture flow depth $y_{50_{TWL}}$ to y_{90} (*c*) relation of TWL length-scale $\mathcal{H}$ to y_{90}

3.3. *Model parameters related to $\overline{c}_{TBL}$ and $\overline{c}_{TWL}$*

Here, we present estimations of the model parameters related to the air concentration within the TBL and the TWL. An inspection of Eq. (2.1) shows that $\overline{c}_{TBL} = f(\beta, \delta, \overline{c}_{\delta/2})$, of which δ and $\overline{c}_{\delta/2}$ were directly determined from velocity and air concentration measurements, respectively. The Rouse number β reflects the ratio of bubble rise velocity and the strength of turbulence (shear velocity) acting on entrained air bubbles, and consequently defines the mode of entrained air transport. For example, a small Rouse number implies dominant turbulent forces, which thereof results in a large quantity of small air bubbles being transported close to the channel bed, whereas a large Rouse number implies that large air bubbles are being transported next to the free-surface. We find that the described transport modes are dependent on the mean air concentration and that the β-parameters for stepped chutes were slightly larger than those for smooth chutes (Fig. 5*a*), which could be associated to the entrainment of larger air bubbles.

The air concentration of the TWL is described by two parameters $\overline{c}_{TWL} = f(y_{50_{TWL}}, \mathcal{H})$, compare Eq. (2.2), of which the mixture flow depth $y_{50_{TWL}}$ was extracted directly from measurements for most of the data sets. Here, we normalise $y_{50_{TWL}}$ and the length-scale $\mathcal{H}$ with y_{90}, showing their functional dependence on the mean air concentration (Figs. 5*b,c*). We note that the normalisation with y_{90} provided the most clear relationship, which may simply be because $\langle \overline{c} \rangle$ is defined in terms of y_{90} [Eq. (1.1)]. Further, the unique dependence between model parameters and mean air concentration is not completely unexpected, as previous researchers have fitted empirical parameters that only depend on $\langle \overline{c} \rangle$, see for example Chanson (1995); Chanson and Toombes (2001). However, it is remarkable that model parameters of the TWL are similarly well behaved for smooth and stepped chutes, and data scatter is only observed beyond $\langle \overline{c} \rangle \gtrapprox 0.5$ to 0.6. For stepped chutes, the deviation from the linear trend is likely to result from a change in flow regime, i.e., the flow changes from skimming flow to transition flow (Kramer and Chanson 2018).
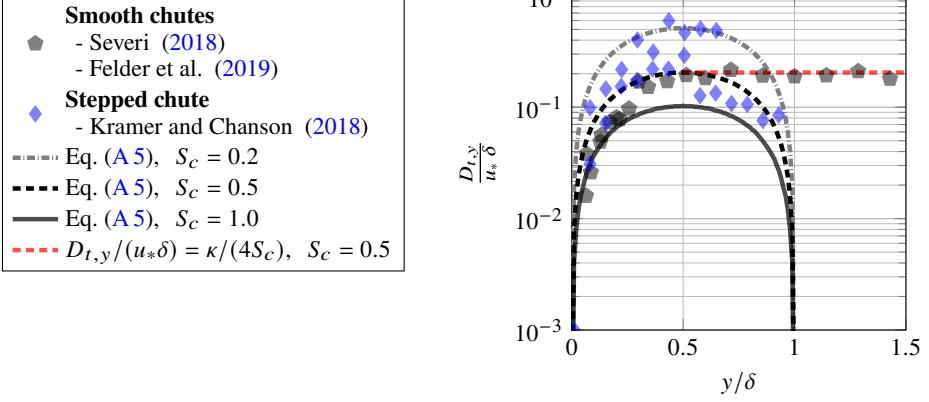
Figure 6: Measured turbulent diffusivities versus theoretical parabolic distribution for different turbulent Schmidt numbers

4. Discussion

4.1. *Turbulent Schmidt number*

In § 3.3, we have discussed the dependence of the depth-averaged parameter β on the mean air concentration. From a Reynolds-Averaged modelling perspective, quantifying the turbulent Schmidt number is of interest since it enables a direct relationship between turbulent momentum diffusivity and turbulent mass diffusivity (Pope 2000; Gualtieri et al. 2017). Hence, we adopt a Reynolds-Averaged form of the advection-diffusion equation for air in water (see also Appendix A, Eq. A 3):

$$\overline{v}_r \, \overline{c} = D_{t,y} \frac{\partial \overline{c}}{\partial y} \tag{4.1}$$

which can be conveniently re-arranged:

$$D_{t,y} = \frac{\overline{v}_r \, \overline{c}}{\partial \overline{c}/\partial y} \tag{4.2}$$

Equation (4.2) allows for a direct evaluation of $D_{t,y}$ from measurements, given that the local air concentrations, their gradients, and bubble rise velocities are known. For selected profiles from Severi (2018), Kramer and Chanson (2018), and Felder et al. (2019), we evaluate $\partial \overline{c}/\partial y$ using a central differences approach, and we characterize bubble sizes from intrusive phase-detection probe measurements by adopting the Sauter diameter $d = 6\,\overline{c}/a = 1.5\overline{u}\,\overline{c}/F$ (Ishii and Hibiki 2011; Hohermuth et al. 2021), where $a = 4F/\overline{u}$ is the interfacial area per volume of air water mixture (Cummings 1996, Eq. 4.6.13), and F is the particle count rate. We estimate still water rise velocities ($\overline{v}_0$) for bubbles with 1 mm $< d <$ 10 mm using the approach of Clift et al. (1978, Eq. 7-3), which we correct for gravity slope and concentration effects after Chanson (1995, 1996) as $\overline{v}_r = \overline{v}_0 \cos(\theta)\sqrt{1 - \overline{c}}$. In a next step, we compute turbulent diffusivities through Eq. (4.2), which are compared against the boundary layer thickness in Fig. 6.

We consider the classical parabolic turbulent diffusivity distribution (Eq. A 5) for different S_c-values, which allows us to conclude that the turbulent Schmidt number for air water flows ranges between 0.2 and 1.0 (compare Fig. 6), which is well in accordance with published literature values for turbulent mass transfer in other environmental flows (Gualtieri et al. 2017). Lastly, the re-analysed smooth chute data suggests that the turbulent diffusivity

becomes constant for $y > \delta/2$ (red dotted line), similar to other open-channel flows (Coleman 1970; Dey 2014). Based on this finding and reasons outlined in Appendix A, we had already adopted a parabolic-constant diffusivity distribution, splitting the expression for the air concentration within the TBL into two parts, separated by $\delta/2$ (see Eq. 2.1).

4.2. *Comparison with other models and limitations*

The determination of the four (five) free physical parameters of the convoluted two-state air concentration profile was outlined in § 2.4. Naturally, the number of free parameters is larger than for commonly used single-layer models, e.g., Chanson and Toombes (2001, Eq. 4.1, two free parameters), and comparable to other double layer-models, e.g., Straub and Anderson (1958, four free parameters). However, the introduced parameters respond to physical properties of the flow, and they allow to assess the relative contribution of individual physical momentum processes on the air concentration profile.

Our theoretical profile [Eq. (2.2) for $\langle \overline{c} \rangle \lessgtr 0.25$ and Eq. (2.8) for $\langle \overline{c} \rangle \gtrless 0.25$] was able to characterize the air concentration distribution of all tested data sets (see Supplementary Material), including different flow rates ($q = 0.03$ to 0.92 m^2/s) and flow regimes over smooth and stepped chutes (transition versus skimming flow), with angles ranging from $\theta = 7.5°$ and $75°$. Model parameters of the TBL and TWL were between $\beta = 0.05$ to 1.2 (Fig. 5a) and $\mathcal{H}/y_{90} = 0$ to 1 (Fig. 5c), both showing a unique dependence on the mean air concentration. The transition/interface parameters were determined as $y_\star/\delta = 0.6$ to 0.9 (Fig. 4c) and $\sigma_\star/\delta = 0.1$ to 0.2. Given a measured air concentration distribution, $y_\star$ can also be obtained from $\overline{c}_\star$, where the latter followed an empirical relationship $\overline{c}_\star = 1.37\langle \overline{c} \rangle - 0.14$ (Fig. 4d).

When compared to previous models, one of the main advantages of the two-state model is its *universal applicability*, together with *physically interpretable* model parameters. Previous models rely more heavily on empirical fitting parameters, with application domains being limited to certain chute geometries (smooth versus stepped) or to certain flow regimes (transition versus skimming flow), see for example Chanson and Toombes (2001, Table III-3). Figure 7 compares the convoluted two-state model with common single-layer models for stepped chute data from Bung (2009). All models describe the air concentration reasonably well for $y/y_{90} \gtrless 0.4$, while the models of Wood (1984) and Chanson and Toombes (2001) are upper bounded by $y/y_{90} = 1$. Below $y/y_{90} \lessgtr 0.4$, only the two-state model is able to capture the region which has traditionally been referred to as concentration boundary layer (Chanson 1996), which is due to the novel representation of underlying physical processes.

The present two-state air concentration model has some limitations, which are herein discussed. The parameters $\overline{c}_{\delta/2}$ and δ were directly extracted from original measurements, i.e., no predictive formulas exist, which however does not hinder the physical interpretation of mass transport parameters in self-aerated flows. In our derivations related to the modified Rouse profile for air bubbles in water (Appendix A), we have assumed a constant bubble rise velocity as well as uniform flow conditions. To estimate the effect of a concentration-dependent rise velocity, we derive alternative solutions of the advection-diffusion equation using $\overline{v}_r = \overline{v}_0 \cos(\theta)\sqrt{1 - \overline{c}}$ (Chanson 1995, 1996, Appendix C), where $\overline{v}_0$ is the rise velocity for clear/still water conditions, i.e., $\overline{c} \approx 0$ (similar to § 4.1). Although only marginal differences in resulting concentration profiles were observed (not shown), we cannot rule out that a more detailed assessment of bubble size distributions would help to improve our understanding of the air concentration distribution within the TBL. Related to the uniform equilibrium assumption, our data indicate that Eq. (2.1) is also applicable within the gradually-varied flow region, which is in agreement with previous findings (Chanson 1995).
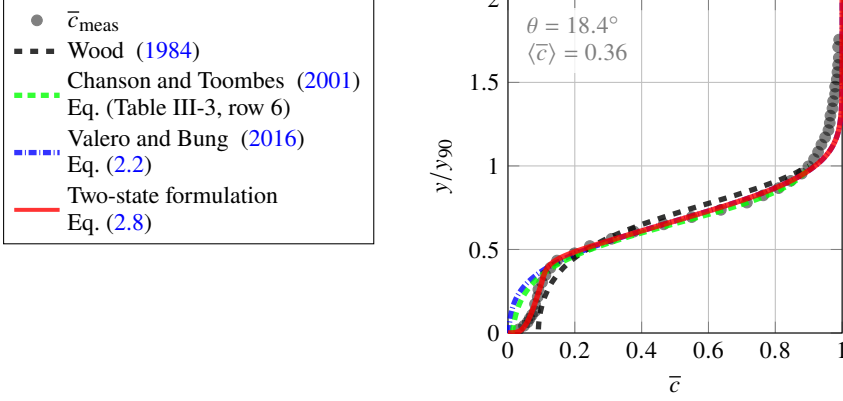
Figure 7: Comparison of the proposed two-state formulation with common air concentration models for stepped chutes; data from Bung (2009) with $q = 0.07$ m^2/s; step height $h = 0.06$ m; measurements taken at step edge 16

5. Conclusion

In this research, we formulate a two-state model to describe air concentration distributions in self-aerated free-surface flows. The rationale behind the model is that the flow can be decomposed into a Turbulent Boundarly Layer (TBL) and a Turbulent Wavy Layer (TWL), featuring a log-law and a constant free-stream velocity, respectively. The corresponding air concentration distributions are mathematically described by a modified Rouse profile and a Gaussian error function, which conceptually implies that the bubbly flow (within the TBL) is driven by high shear and turbulent diffusion, whereas free-surface waves/perturbations of the TWL lead to large concentrations due to voids within wave troughs.

The transition point between the two layers was previously discussed in aerated flow literature (Straub and Anderson 1958), but no physical reasoning was given. Here, we argue that the flow transition corresponds to a time-averaged TBL - TWL interface position that is closely related to the boundary layer thickness. From an instantaneous point of view, the flow takes either a TBL or a TWL state, and the interface position is described by a Gaussian probability density function. Subsequently, a convolution of the two states with the interface probability provides the time-averaged air concentration profile. As such, our model is the first to establish a connection between air concentration and velocity distribution based on physically explainable model parameters.

We test our theoretical air concentration profile against more than 500 experimental concentration profiles from smooth and stepped chute literature data sets. We show that, regardless of the data set, the model is able to capture the profiles and to discern the different air concentration regions contained within. It is noted that laboratory flows with $\langle \overline{c} \rangle \lessgtr 0.25$ are dominated by free-surface aeration/entrapped air, and the air concentration distribution is confined to the TWL. For larger $\langle \overline{c} \rangle$, air bubbles are diffused deeper into the water column, implying that the time-averaged air concentration is described by the convolution of the Rouse profile and the Gaussian error function with the interface probability. We characterize different transport modes of entrained air bubbles (within the TBL) based on the ratio of bubble rise velocity and shear velocity, expressed through the Rouse number β, and we show that the transport mode is a function of the mean air concentration. Model parameters related to the TWL were also explained via the mean air concentration and behaved similarly for smooth and stepped chutes. Finally, we present values of the turbulent Schmidt number in

14

highly aerated flows, which we anticipate to be of high relevance for future numerical model applications based on Reynolds-averaged Navier-Stokes equations.

Author ORCID. M. Kramer, https://orcid.org/0000-0001-5673-2751; D. Valero, https://orcid.org/0000-0002-7127-7547

Appendix A. Modified Rouse profile for air bubbles in water

A governing equation for the bed-normal air concentration distribution can be written by simplifying the advection-diffusion equation for air in water. We assume a two-dimensional steady flow, where the air concentration only varies in bed-normal, but not in streamwise (x) or transverse (z) direction. Therefore, the following gradients can be neglected $\partial(\cdot)/\partial t = 0$, $\partial(\cdot)/\partial x = 0$, $\partial(\cdot)/\partial z = 0$, and the advection-diffusion equation reduces to:

$$\frac{\partial(\overline{v}_r \, \overline{c})}{\partial y} = \frac{\partial}{\partial y}\left(D_{t,y}\frac{\partial\overline{c}}{\partial y}\right) \tag{A 1}$$

where $\overline{v}_r$ is the rise velocity of air bubbles, which is defined positive in bed-normal direction, $\overline{c}$ is the volumetric air concentration (volume of air/total volume), and $D_{t,y}$ is the turbulent diffusivity. We note that the full derivation of the generalized advection-diffusion equation, including Reynolds-Averaging and gradient diffusion theory, is presented, amongst others, in Dey (2014). A first integration of Eq. (A 1) leads to:

$$\int \frac{\partial}{\partial y}\left(\overline{v}_r \, \overline{c}\right)\mathrm{d}y = \int \frac{\partial}{\partial y}\left(D_{t,y}\frac{\partial\overline{c}}{\partial y}\right)\mathrm{d}y \tag{A 2}$$

$$\overline{v}_r \, \overline{c} = D_{t,y}\frac{\partial\overline{c}}{\partial y} + \mathcal{K}_1 \tag{A 3}$$

To simplify Eq. (A 3), the partial differential is replaced by the total differential, only the first set of solutions ($\mathcal{K}_1 = 0$) is considered, and a constant rise velocity is assumed. Separating variables and performing a second integration from an arbitrary elevation y to $\delta/2$ yields:

$$\int_{\overline{c}}^{\overline{c}_{\delta/2}} \frac{1}{\overline{c}}\,\mathrm{d}\overline{c} = \overline{v}_r \int_y^{\delta/2} \frac{1}{D_{t,y}}\mathrm{d}y \tag{A 4}$$

Now, we invoke a parabolic distribution of turbulent diffusivity (likewise Rouse 1961):

$$D_{t,y} = \frac{\kappa u_* y}{S_c}\left(1 - \frac{y}{\delta}\right) \tag{A 5}$$

where κ is the von Kármán constant, u_* is the friction velocity, and S_c (= $\nu_t/D_{t,y}$) is the turbulent Schmidt number, defined as the ratio of eddy viscosity ν_t (i.e., momentum diffusivity) and turbulent mass diffusivity. Substitution and integration of Eq. (A 4) gives:

$$\frac{\overline{c}}{\overline{c}_{\delta/2}} = \exp\left(\frac{\overline{v}_r S_c}{\kappa u_*} \ln\left[\frac{1}{\frac{\delta}{y}-1}\right]\right) \tag{A 6}$$

which simplifies to:

$$\overline{c}(y) = \overline{c}_{\delta/2}\left(\frac{y}{\delta-y}\right)^{\beta}, \quad y \leqslant \delta/2 \tag{A 7}$$

where $\beta = \overline{v}_r S_c/(\kappa u_*)$ is the Rouse number. It is noted that S_c is assumed constant and Eq. (A 7) is similar to the well-known Rouse equation for sediment transport but incorporating subtle differences, which are: (1) a positively defined bubble rise velocity, (2) a change of integration limits, and (3) a use of the boundary layer thickness δ instead of the water depth. The parameter S_c was encapsulated within β, for convenience.

We note that a purely parabolic diffusivity profile (Eq. A 5) becomes negative for $y_i/\delta > 1$, which could occasionally happen if σ_* is large. The next appropriate choice is a parabolic-constant diffusivity distribution, which has been used for suspended sediment transport (Coleman 1970; Dey 2014), and which we also observe in Fig. 6, where the turbulent diffusivity $D_{t,y}$ becomes independent of y. Adopting a constant $D_{t,y}(\delta/2) = \kappa u_* \delta/(4S_c)$ for $y > \delta/2$, we integrate Eq. (A 3) between $\delta/2$ and an arbitrary elevation:

$$\int_{\overline{c}_{\delta/2}}^{\overline{c}} \frac{1}{\overline{c}}\,\mathrm{d}\overline{c} = \overline{v}_r \int_{\delta/2}^{y} \frac{4S_c}{\kappa u_* \delta}\mathrm{d}y \tag{A 8}$$

yielding the following exponential distribution:

$$\overline{c}(y) = \overline{c}_{\delta/2}\exp\left(\frac{4\beta}{\delta}\left(y-\frac{\delta}{2}\right)\right), \quad y > \delta/2 \tag{A 9}$$

REFERENCES

BAI, R. AND TANG, R. AND WANG, H. 2022 Closure to 'Case tdudy of prototype hydraulic jump on slope: Air entrainment and free-surface measurement' by Zhongtian Bai, Ruidi Bai, Rongcai Tang, Hang Wang, and Shanjun Liu. *J. Hydraul. Res.* **148** (11), 07022007.

BROCCHINI, M. AND PEREGRINE, D. H. 2022 The dynamics of strong turbulence at free surfaces. Part 1. Description. *J. Fluid Mech.* **449**, 225–254.

BOES, R. 2000 Two-phase flow and energy dissipation at large cascades (in German). Phd Thesis, ETH Zurich.

BUNG, D. 2009 Zur selbstbelüfteten Gerinneströmung auf Kaskaden mit gemäßigter Neigung (in German), Phd Thesis, University of Wuppertal.

CASTRO-ORGAZ, O. AND HAGER, W. 2010 Drawdown curve and turbulent boundary layer development for chute flow. *J. Hydraul. Res.* **48** (5), 591–602.

CHAN, W. R. C. AND JOHNSON, P. L. AND MOIN, P. 2021 The turbulent bubble break-up cascade. Part 1. Theoretical development. *J. Fluid Mech.* **912**, A42.

CHANSON, H. 1994 Drag reduction in open-channel flow by aeration and suspended load. *J. Hydraul. Res.*, **32** (1), 87–101.

CHANSON, H. 1995 Air bubble diffusion in supercritical open channel flow. In *Proceedings of the 12th Australasian fluid mechanics conference (AFMC), Sydney, Australia*, pp. 707-–710. Australasian fluid mechanics conference.

CHANSON, H. 1996 Air bubble-entrainment in free surface turbulent shear flows. Academic Press.

CHANSON, H. AND TOOMBES, L. 2001 Experimental investigations of air entrainment in transition and

skimming flows down a stepped chute. Application to embankment overflow stepped spillways. *Research Report No. CE158*. Dept. of Civil Engineering, The University of Queensland, Brisbane.

CLIFT, R. AND GRACE, J. R. AND WEBER, M. E. 1978 Bubbles, Drops, and Particles. *Academic Press*.

COLEMAN, N. L. 1970 Flume studies of the sediment transfer coefficient. *Water Resour. Res.* **6** (3), 801–809.

CUMMINGS, P. D. 1996 Aeration due to breaking waves. Phd Thesis, *Department of Civil Engineering, The University of Queensland, Brisbane*.

DEANE, G. B. AND STOKES, M D. 2002 Scale dependence of bubble creation mechanisms in breaking waves, *Nature* **418** (6900), 839–844.

DEY, S. 2014 Fluvial Hydrodynamics, *Springer*.

FALVEY, H. T. 1990 Cavitation in chutes and spillways. Engineering Monograph No. 42. United States Department of the Interior, Bureau of Reclamation

FELDER, S., HOHERMUTH, B. AND BOES, R. M. 2019 High-velocity air-water flows downstream of sluice gates including selection of optimum phase-detection probe. *Int. J. Multiphase Flow* **116**, 203–220.

FELDER, S. AND SEVERI, A. AND KRAMER, M. 2022 Self-aeration and flow resistance in high-velocity flows down spillways with micro-rough inverts. *J. Hydraul. Engng* **149** (6), 04023011.

FRIZELL, K. W. AND RENNA, F. M. AND MATOS, J. 2013 Cavitation potential of flow on stepped spillways. *J. Hydraul. Engng* **139** (6), 630–636.

GUALTIERI, C. AND ANGELOUDIS, A. AND BOMBARDELLI, F. AND JHA, S. AND STOESSER, T. 2017. On the values for the turbulent Schmidt number in environmental flows. *Fluids* **2** (2), 17.

GULLIVER, J. S., THENE, J. R., AND RINDELS, A. J. 1990 Indexing gas transfer in self-aerated flows. *Journal Environ. Engng* **116** (3), 503–523.

HAGER, W. H 1991 Uniform aerated chute flow. *J. Hydraul. Engng* **117** (4), 528–533.

HOHERMUTH, B. AND KRAMER, M. AND FELDER, S. AND VALERO, D. 2021 Velocity bias in intrusive gas-liquid flow measurements. *Nat. Commun.* **12**, 4123.

HOHERMUTH, B. BOES, R. AND FELDER, S. 2021 High-velocity air-water flow measurements in a prototype tunnel chute: scaling of void fraction and interfacial velocity. *J. Hydraul. Engng* **147** (11), 04021044.

ISHII, M. AND HIBIKI, T. 2011 *Thermo-fluid dynamics of two-phase flow*, Springer, 2nd edn. Springer.

KILLEN, J. M. 1968 The surface characteristics of self aerated flow in steep channels. Phd Thesis, *University of Minnesota*, Minneapolis, MN.

KRAMER, M. AND CHANSON, H. 2018 Transition flow regime on stepped spillways: air–water flow characteristics and step-cavity fluctuations. *Environ. Fluid Mech.* **18** (4), 947–965.

KRAMER, M. AND HOHERMUTH, B. AND VALERO, D. AND FELDER, S. 2020 Best practices for velocity estimations in highly aerated flows with dual-tip phase-detection probes. *Int. J. Multiphase Flow* **126**, 103228.

KRAMER, M. AND FELDER, S. AND HOHERMUTH, B. AND VALERO, D. 2018 Drag reduction in aerated chute flow: Role of bottom air concentration. *J. Hydraul. Engng* **147** (11), 04021041.

KRUG, D. AND PHILIP, J. AND MARUSIC, I. 2017 Revisiting the law of the wake in wall turbulence. *J. Fluid Mech.* **811**, 421–435.

LANE, E. W. 1939 Entrainment of air in swiftly flowing water. *Civil Engrs* **9** (2), 89–96.

MARUSIC, I. AND MCKEON, B.J. AND MONKEWITZ P.A. AND NAGIB, H.M. AND SMITS, A.J. AND SREENIVASAN, K.R.. 2008 Wall-bounded flows at high Reynolds numbers: Recent advances and key issues. *Phys. Fluids* **22**, 065103.

MORRILL-WINTER, C. AND PHILIP J. AND KLEWICKI, J. 2017 An invariant representation of mean inertia: theoretical basis for a log law in turbulent boundary layers. *J. Fluid Mech.* **813**, 594–617.

NAGIB, H. M. AND CHAUHAN, K. A. 2008 Variations of von Kármán coefficient in canonical flows. *Phys. Fluids* **20**, 101518.

PLEIZIER, N. K. AND ALGERA, D. AND COOKE, S. J. AND BRAUNER, C. J. 2020 A meta-analysis of gas bubble trauma in fish. *Fish Fisheries* **21** (6), 1175–1194.

POPE, S. B. 2000 *Turbulent Flows*, Cambridge University Press.

RAO, N.S.L. AND GANGADHARAIAH, T. 1971 Distribution characteristics of self-aerated flows. *Characteristics of self-aerated free-surface flows. water and waste water/current research and practice* **10**, 119-161.

ROUSE, H. 1961 *Fluid mechanics for hydraulic engineers*. Dover.

SEVERI, A. 2018 Aeration performance and flow resistance in high-Velocity flows over moderately sloped spillways with micro-rough bed. Phd Thesis Water Research Laboratory, School of Civil and Environmental Engineering, UNSW Sydney, 345 pages.

STRAUB, L. AND ANDERSON, A. G. 1958 Experiments on self-aerated flow in open channels. *J. Hydraul. Division* **84** (7), 1–35.

VALERO, D. AND BUNG, D. 2016 Development of the interfacial air layer in the non-aerated region of high-velocity spillway flows. Instabilities growth, entrapped air and influence on the self-aeration onset. *Int. J. Multiphase Flow* **84**. 66–74.

VALERO, D. AND BUNG, D. 2018 Reformulating self-aeration in hydraulic structures: Turbulent growth of free surface perturbations leading to air entrainment. *Int. J. Multiphase Flow* **100**, 127–142.

WEI, W. 2022 Free surface aeration and development dependence in chute flows, *Sci Rep* **12**, 1477.

WEI, W. AND XU, W. AND DENG, J. AND GUO, Y. 2022 Self-aeration development and fully cross-sectional air diffusion in high-speed open channel flows. *J. Hydraul. Res.* **60** (3), 445–459.

WILHELMS, S. AND GULLIVER, J. S. 2005 Bubbles and waves description of self-aerated spillway flow. *J. Hydraul. Res.* **43** (5), 522–531.

WOOD, I. 1984 Air entrainment in high speed flows. In *Proceedings of the international symposium on scale effects in modelling hydraulic structures* paper 4, IAHR.

ZHANG, G. 2017 Free-surface aeration, turbulence, and energy dissipation on stepped chutes with triangular steps, chamfered steps, and partially blocked step cavities. Phd Thesis, School of Civil Engineering, The University of Queensland.

ZHANG, G. AND CHANSON, H. 2017 Self-aeration in the rapidly- and gradually-varying flow regions of steep smooth and stepped spillways. *Environ. Fluid Mech.* **17**, 27–46.